ECCOMAS Congress 2016
VII European Congress on Computational Methods in Applied Sciences and Engineering
M. Papadrakakis, V. Papadopoulos, G. Stefanou, V. Plevris (eds.)
Crete Island, Greece, 5–10 June 2016

ON THE REGULARISATION OF NON-REFLECTING BOUNDARY CONDITIONS NEAR ACOUSTIC RESONANCE

Christian Frey, Hans-Peter Kersken

German Aerospace Center (DLR)
Linder Hohe, 51147 Cologne, Germany
e-mail: christian.frey@dlr.de, hans-peter.kersken@dlr.de

Keywords: Nonreflecting Boundary Conditions, Acoustic Resonance, Turbomachinery Flutter

Abstract. *In this paper we discuss the phenomenon of acoustic resonance in the context of non-reflecting boundary conditions and its impact on the analysis of turbomachinery blade flutter. Acoustic resonance is observed on the one hand when flutter curves, i.e., the aerodynamic damping as a function of the interblade phase angle, displays singularities at certain angles. On the other hand, the implementation of appropriate inlet and outlet boundary conditions naturally leads to the normal mode analysis of the Euler equations on eiher cylindrical (2D) or annular ducts (3D). To formulate boundary conditions one typically carries out the normal mode analysis and thus decomposes the space of normal modes as a direct sum of incoming and outgoing modes. This decomposition, however, breaks down when the generalised eigenvalue problem no longer produces a complete set of eigenvectors and one obtains non-trivial Jordan blocks. Both phenomena are shown to be due to acoustic modes with vanishing normal group velocity.*

The main goal of this paper is to outline how the numerical boundary conditions can be regularised near acoustic resonance. The impact of this regularisation on the prediction of flutter stability is then demonstrated. Moreover, we interpret the regularisation as an interpolation between the exact non-reflecting and the approximative characteristic, one-dimensional boundary conditions.

INTRODUCTON

The design of modern turbomachinery increasingly relies on unsteady flow simulations, especially to avoid engine failure due to blade flutter. Typically, the flutter analysis is based on the prediction of the unsteady flow response for a forced motion of the blades at various operating conditions [1]. Usually, this forced motion is defined by the structural displacement, q^{s}, corresponding to a structural eigenmode ψ,

$$q^{\mathrm{s}}(t,x) = \mathrm{Re}\left[q^{\mathrm{s}}_{\mathrm{mod}}(t)\psi(x)\right],$$

where the modal displacement is the harmonic oscillation

$$q^{\mathrm{s}}_{\mathrm{mod}}(t) = e^{\mathrm{i}\omega t},$$

with the angular frequency ω being the eigenfrequency $\sqrt{k/m}$. From the unsteady pressure on the blade surface one can determine the aerodynamic damping,

$$\delta = -\frac{\mathrm{Re}\, W_{\mathrm{cyc}}}{\omega^2 m}, \quad W_{\mathrm{cyc}} = \int_0^{2\pi/\omega}\int_\Gamma \left(\dot{q}^{\mathrm{s}}_{\mathrm{mod}}(t)\psi(x)\right)^H \left(p(t,x)\vec{n}(t,x)\right) dS(x)dt, \tag{1}$$

and thus estimate if the coupled system is stable at rest. Whereas the real part of W_{cyc} represents the net work per period done on the structure by the unsteady flow, the imaginary part of W_{cyc} gives rise to the aerodynamic stiffness coefficient

$$\kappa = \frac{\mathrm{Im}\, W_{\mathrm{cyc}}}{\omega^2 m},$$

from which a frequency shift of the coupled fluid structure system can be determined. One

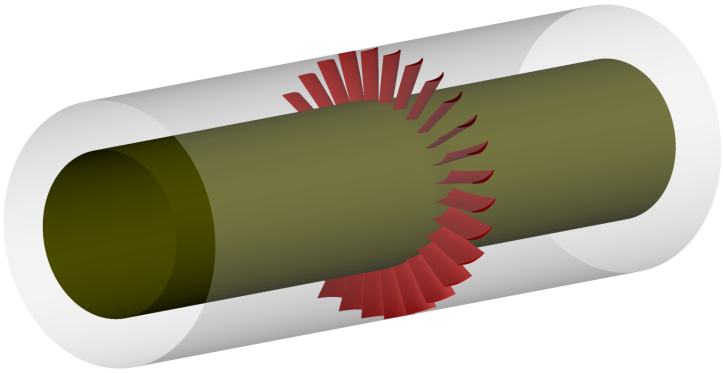

Figure 1: Idealised flow domain for the anaylsis of blade flutter

usually considers an idealised flow domain as in Fig. 1, i.e., the interactions with neighbouring blade rows are neglected.

Under the assumption that the blade row consists of N structurally uncoupled blades, each eigenmode ψ that one obtains from the structural analysis of one blade, gives rise to the full annulus modes

$$(\psi, e^{\mathrm{i}\sigma}\psi, e^{2\mathrm{i}\sigma}\psi, \ldots, e^{(N-1)\mathrm{i}\sigma}\psi),$$

where the n-th component represents the mode shape of the n-th blade, and $\sigma \in [-\pi, \pi)$ is such that $N\sigma = 2\pi$. σ is called the *interblade phase angle*. The integer

$$N_\mathrm{d} = \frac{2\pi}{\sigma}$$

is called the *nodal diameter*. A full annulus mode has an interblade phase angle of σ if the modal displacement of the blade n lags that of blade $n+1$ by a time shift of σ/ω. In this case the unsteady flow response $q(t, x)$ will exhibit the same space time symmetry, i.e.,

$$q(t, x, r, \vartheta + 2\pi/N) = q(t + \sigma/\omega, x, r, \vartheta),$$

Together with (1) one deduces that blade vibrations of different interblade phase angles are uncoupled. Therefore, one usually computes the aerodynamic damping for each interblade phase angle. The result is plotted in the so-called *damping curve*, although, strictly speaking, it consists of a discrete set of N values.

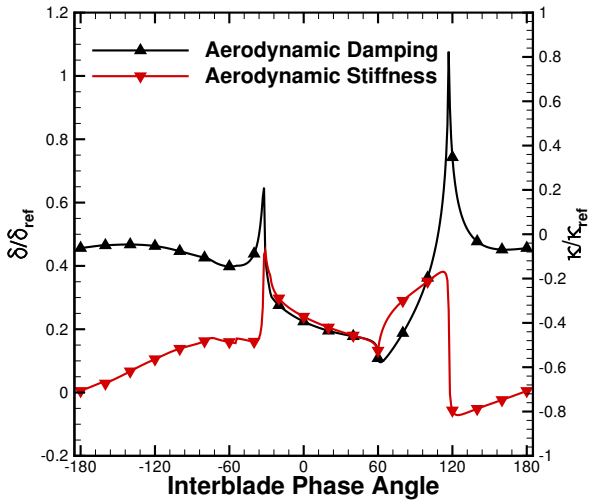

Figure 2: Aerodynamic damping and stiffness over interblade phase angle for a compressor blade.

Figure 2 shows the aerodynamic damping and stiffness curves for the academic compressor test case Standard Configuration 10, cf. [2]. The unsteady flow response is computed using the time-linearised approach [3, 4]. One observes that the damping appears to be "smooth" except for a few interblade phase angles.

It is easy to see that the flutter curve corresponds to the discrete Fourier transform of the influence coefficients, i.e., the modal forces on one blade which are due to the vibration of another one [5]. In many cases, the influence coefficents decay rapidly as the distance between two blades of the blade row increases and one obtains smooth flutter curves. For instance, if the influence coefficients of all but direct neighbours can be neglected the flutter curve can be approximated rather accurately by a function $\tilde{\delta}(\sigma) = c_0 + c_1 \cos(\sigma - \sigma_1)$, cf. [6]. However, this may not always be the case, as the spikes and the sudden drops in the curves in Fig. 2 show. When these singularities are observed near a minimum damping close to zero, the CFD based prediction of flutter stability becomes questionable, as the infinite slope of the flutter curve indicates a considerable uncertainty in the damping.

The occurence of these singularities is due to the phenomenon of *acoustic resonance* [6]. One speaks of acoustic resonance if a flow unsteadiness, in this case caused by a vibrating blade, is resonant with an acoustic wave whose energy does not propagate out of the configuration. As is well-known, the energy transport of a wave is closely related to its group velocity. For such a standing wave to be excited it is also necessary that the unsteadiness has the same circumferential wave number (or nodal diameter) as the acoustic mode. Consequently, one observes acoustic resonance only at certain interblade phase angles. In turbomachinery, acoustic resonance can occur at specific operating conditions. Often the source of the instability unknown. Alongside blade vibration possible sources of excitation include pressure disturbances due to the periodic blade passings, rotating instabilities and vortex shedding. For acoustic resonances observed during turbomachinery experiments, the reader is refered to [7, 8] and the literature cited therein.

The goal of this work is to study the issue of acoustic resonance in the context of non-reflecting boundary conditions. When acoustic resonance occurs, there no longer exists a complete set of duct eigenmodes so that the standard formulations of inlet and outlet boundary conditions (see e.g. [9, 10]) are no longer possible.

The paper is organised as follows. First we revisit the theory of non-reflecting boundary conditions for the linearised Euler equations. Then we show how to regularise the boundary conditions by shifting the frequency slightly to the complex lower half plane. This technique has been used by Moinier and Giles [11] to simplify the determination of the propagation direction of normal modes computed numerically. We demonstrate the impact of the regularisation on the prediction of flutter stability by means of a compressor blade. It is shown that the regularisation has the effect of a mollifier for the flutter curves. Most of the mathematical arguments carry over to symmetrisable hyperbolic problems. Therefore, we will use general arguments whenever possible.

We interpret the regularisation as an interpolation between the exact non-reflecting and the characteristic boundary conditions. Since two-dimensional non-reflecting boundary conditions are typically used for three-dimensional turbomachinery configurations, we discuss the question to what extent the results obtained with two-dimensional boundary conditions are representative in real applications.

1 NON-REFLECTING BOUNDARY CONDITIONS

We consider the Euler equations in $\mathbb{R}^n$ in conservative variables $q = (\rho, \rho U, \rho e_\mathrm{t})$

$$\frac{\partial q}{\partial t} + \operatorname{div} F(q) = 0 \tag{1.1}$$

with the inviscid flux

$$F(q) = \begin{pmatrix} \rho U \\ \rho U \otimes U + p\,\mathrm{Id} \\ \rho U h_\mathrm{t} \end{pmatrix}.$$

It is well-known that the Euler equations form a symmetrisable hyperbolic system of conservation laws [12]. In particular, the Hessian of the entropy density, viewed as a function

$$(\rho, \rho U, \rho e_\mathrm{t}) \to -\rho s,$$

is a symmetriser, i.e.,

$$T(q) = \left(\frac{\partial^2(-\rho s)}{\partial q_i \partial q_j}\Big|_q \right)_{i,j}$$

is symmetric positive definite and $T(q)\frac{\partial F^k}{\partial q}|_q$ is symmetric for all q and k. Assume that the computational domain is the half space $(-\infty, 0) \times \mathbb{R}^{n-1}$ and that the solution is periodic in the $n-1$ tangential variables. Consider the linearised equations at some mean flow conditions, e.g., the area average of the conservative variables. Transformation of the linearised equations into the frequency and wave number domain thus yields a linear system for $\hat{q}_{\omega,\xi}$,

$$\left(\omega + \sum_k \xi_k \frac{\partial F^k}{\partial q}\right) \hat{q}_{\omega,\xi} = 0. \tag{1.2}$$

The matrix on the left-hand side is symmetric with respect to the inner product defined by T and, up to a factor i, equals the principal symbol [13]. Its determinant is a homogeneous polynomial of degree $n+2$ in $(\omega, \xi) \in \mathbb{R}^{n+1}$, whose zeros form the so-called characteristic variety $\mathscr{C}$, cf. [14]. Suppose that at a certain point $(\omega, \xi) \in \mathscr{C}$ the characteristic variety is smooth and that the lines $\xi = \text{const}$ are, near (ω, ξ), transversal to $\mathscr{C}$. Then, the angular frequency ω such that Eqn. (1.2) has a non-trivial solution, can be written locally as a function of ξ, and the *group velocity* is then defined by

$$v_{\mathrm{g}}(\omega, \xi) = -\frac{\partial \omega}{\partial \xi}. \tag{1.3}$$

The Euler equations for an ideal gas can be rewritten in primitive variables, $q_{\mathrm{prim}} = (\rho, U, p)$,

$$\frac{\partial q_{\mathrm{prim}}}{\partial t} + \sum_j A^j \frac{\partial q_{\mathrm{prim}}}{\partial x^j} = 0$$

where

$$A^j = U^j \,\mathrm{Id} + \begin{pmatrix} 0 & \rho e_j^T & 0 \\ 0 & 0 & \rho^{-1} e_j \\ 0 & \gamma p e_j^T & 0 \end{pmatrix},$$

and $e_1, \ldots, e_n$ is the standard basis of $\mathbb{R}^n$. The characteristic variety of the linearised Euler equations is thus given by those (ω, ξ) satisfying

$$(\omega + \xi \cdot U)^n ((\omega + \xi \cdot U)^2 - a^2 \|\xi\|^2) = 0. \tag{1.4}$$

In primitive variables, the convective modes

$$r_1 = \begin{pmatrix} \rho \\ 0 \\ 0 \end{pmatrix}, \quad r_2 = \begin{pmatrix} 0 \\ a e_1 \\ 0 \end{pmatrix}, \ldots r_n = \begin{pmatrix} 0 \\ a e_{n-1} \\ 0 \end{pmatrix}, \tag{1.5}$$

together with the acoustic eigenvectors

$$r_{n+1} = \begin{pmatrix} \rho \\ a\frac{\xi}{\|\xi\|} \\ \gamma p \end{pmatrix}, \quad r_{n+2} = \begin{pmatrix} \rho \\ -a\frac{\xi}{\|\xi\|} \\ \gamma p \end{pmatrix}, \tag{1.6}$$

thus form a basis of eigenvectors for a given $\xi \in \mathbb{R}^n$. The convective modes correspond to the hyperplane $\omega + \xi \cdot U = 0$, and their group velocity is the flow velocity. The acoustic angular frequencies and wave numbers lie on the oblique cone $(\omega + \xi \cdot U)^2 - a^2 \|\xi\|^2 = 0$. Observe that the acoustic angular frequencies are

$$\omega_{n+1} = -\xi \cdot U - a\|\xi\|, \quad \omega_{n+2} = -\xi \cdot U + a\|\xi\|.$$

We note that the acoustic eigenvalues are simple except for $\xi = 0$.

For the non-reflecting boundary conditions, we consider Eqn. (1.2) as a generalised eigenvalue problem for ξ_1. We will denote the tangential parts of vectors by primed variables, so, for instance,

$$x = (x^1, x'), \quad \xi = (\xi_1, \xi'), \quad A = (A^1, A').$$

For simplicity we will assume that the flow is normally subsonic, $M_1 < 1$, and that the boundary $x_1 = 0$ is an outlet of the domain $\{x_1 < 0\}$, i.e., $M_1 > 0$. The case of an inlet can be treated analogously. In primitive variables, the generalised eigenvalue problem for ξ_1 thus reads

$$\left(\xi_1 A^1 - (-\omega - \xi' \cdot A')\right) r = 0, \tag{1.7}$$

with r being a generalised right-eigenvector. Assume that a complete basis of eigenvectors

$$r_1(\omega, \xi'), \ldots, r_{n+2}(\omega, \xi'),$$

exists for (ω, ξ'), and that the corresponding eigenvalues ξ_1 are, at least locally, smooth functions of ω. Then the boundary conditions can be formulated in terms of the temporal and spatial Fourier coefficients of the flow along the boundary $x_1 = 0$ as follows. Decompose the Fourier coefficients $\hat{q}_{\omega,\xi'}$ into normal modes, i.e.,

$$\hat{q}_{\omega,\xi'} = \sum_{j}^{n+2} \hat{q}^j_{\omega,\xi',\mathrm{mod}} r_j(\omega, \xi').$$

The non-reflecting boundary conditions are satisfied if $\hat{q}^j_{\omega,\xi',\mathrm{mod}} = 0$ for all j such that r_j corresponds to an incoming mode. In case the generalised eigenvalue ξ_1 is a non-zero real and ω is locally a smooth function of ξ_1, the sign of the normal group velocity $-\frac{\partial \omega}{\partial \xi_1}$ can be taken as a criterion to classify the modes into incoming and outgoing ones [14].

Note that the generalised eigenvalue problem is indefinite, since the flux Jacobian $\frac{\partial F^1}{\partial q}$ is indefinite, if the flow is normally subsonic. Therefore, one cannot expect that a basis of eigenvectors exists for all (ω, ξ'). In fact, the cone

$$(\omega + \xi \cdot U)^2 - a^2 \|\xi\|^2 = 0 \tag{1.8}$$

may or may not intersect the line defined by some fixed ω and ξ'. In case the corresponding quadratic equation for ξ_1 has negative discriminant, it will have two complex conjugate solutions. These so-called *cut-off* modes are viewed as incoming if they decrease exponentially at $-\infty$, i.e., if $\operatorname{Im} \xi_1 < 0$. Accordingly, a cut-off mode is called outgoing if $\operatorname{Im} \xi_1 > 0$.

The corresponding (real or complex) eigenvectors are used to define the spectral projections onto the incoming along the outgoing eigenmodes, P_{inc}. The physical boundary condition can thus be written

$$P_{\mathrm{inc}} \hat{q}_{\omega,\xi'} = 0.$$

where

$$P_{\mathrm{inc}} = P_{\mathrm{inc}}(q, \omega, \xi') = R(q, \omega, \xi')^{-1} \begin{pmatrix} 0 & 0 \\ 0 & \mathrm{Id} \end{pmatrix} R(q, \omega, \xi')$$

where the dimensions of the subblocks of the block matrix are given by the number of right and left runnning modes, respectively. The first columns of the right-eigenvector matrix $R(q, \omega, \xi')$ are the left-running eigenvectors of the generalised eigenvalue problem (1.7), the last columns are given by the left-running eigenvectors.

Special care has to be taken in order to define the acoustic eigenvectors. Here, we write the acoustic normal wave numbers as functions of q, ω, and ξ',

$$\xi_{1,\mathrm{a},\pm} = \begin{cases} \pm\frac{\mathrm{i}\|\xi'\|}{\sqrt{1-M_1^2}}, & \text{if } \widetilde{\omega}+\xi'\cdot M' = 0, \\ (M_1 \mp \sqrt{\Delta})\left(\frac{\widetilde{\omega}+\xi'\cdot M'}{1-M_1^2}\right), & \text{if } \widetilde{\omega}+\xi'\cdot M' \neq 0, \quad \Delta \geq 0, \\ (M_1 \pm \mathrm{i}\,\mathrm{sign}(\widetilde{\omega}+\xi'\cdot M')\sqrt{-\Delta})\left(\frac{\widetilde{\omega}+\xi'\cdot M'}{1-M_1^2}\right), & \text{if } \widetilde{\omega}+\xi'\cdot M' \neq 0, \quad \Delta < 0, \end{cases} \tag{1.9}$$

where $\widetilde{\omega} = \omega/a$, $\vec{M} = (M_1, M') = U/a$ and Δ is the discriminant of the corresponding quadratic equation for ξ_1, i.e.,

$$\Delta = 1 - \frac{1-M_1^2}{(\widetilde{\omega}+\xi' M')^2}\|\xi'\|^2.$$

The definition of $\xi_{1,\mathrm{a},\pm}$ ensures that $\operatorname{sign}\operatorname{Im}\xi_{1,\mathrm{a},\pm} = \pm 1$, if $\Delta < 0$. Moreover, it is straightforward to check that

$$\frac{\partial \xi_{1,\mathrm{a},\pm}}{\partial \omega} = \mp\frac{1}{(1-M_1^2)\sqrt{\Delta}}$$

for cut-on modes, i.e., $\Delta > 0$. Therefore, the x^1-group velocity

$$v_{\mathrm{g}}^1(\omega, \xi_{1,\mathrm{a},\pm}, \xi') = -\frac{\partial\omega}{\partial\xi_1}\Big|_{(\xi_{1,\mathrm{a},\pm},\xi')} = -\left(\frac{\partial\xi_{1,\mathrm{a},\pm}}{\partial\omega}\Big|_{(\omega,\xi')}\right)^{-1}$$

is positive for $\xi_{1,\mathrm{a},+}$ and negative for $\xi_{1,\mathrm{a},-}$. The acoustic eigenvectors can be defined by

$$r_{\mathrm{a},\pm}(q,\omega,\xi') = \begin{pmatrix} \rho \\ -\frac{a\xi_\pm}{\omega+\xi_\pm\cdot\vec{M}} \\ \gamma p \end{pmatrix} \tag{1.10}$$

where $\xi_\pm = (\xi_{1,\mathrm{a},\pm}, \xi')$.

The Characteristic Variety

Let us express the characteristic variety in terms of the (directional) Mach numbers and the normalised frequency,

$$\vec{M} = (M_1, \ldots, M_n), \quad M_i = U_i/a, \quad M = \|\vec{M}\|, \quad \widetilde{\omega} = \omega/a.$$

As we have seen above the characteristic variety for the n-dimensional linearised Euler equations consists of:

- The plane $\widetilde{\omega} = -\sum_i M_i\xi_i$, corresponding to the convective modes.
- The cone

$$\left(\widetilde{\omega} + \vec{M}\cdot\xi\right)^2 = \|\xi\|^2. \tag{1.11}$$

  corresponding to acoustic modes.

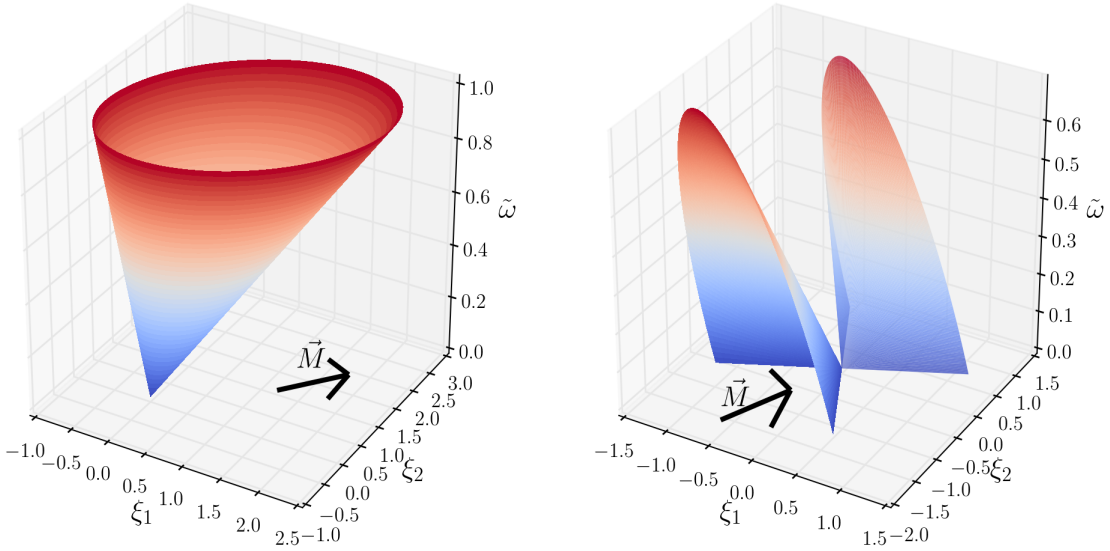

(a) $M = 0.7$, $\alpha = 55°$.

(b) $M = 1.5$, $M_x = 0.5$.

Figure 3: Characteristic varieties for subsonic and supersonic cases.

To analyse the cone (1.11), consider an orthonormal basis $(\widetilde{e}_1, \ldots, \widetilde{e}_n)$ such that

$$\vec{M} = M\widetilde{e}_1.$$

Then, with respect to this basis, Eqn. (1.11) takes the form

$$(1 - M^2)\widetilde{\xi}_1^2 - 2M\widetilde{\omega}\widetilde{\xi}_1 + \sum_{i \neq 1} \widetilde{\xi}_i^2 - \widetilde{\omega}^2 = 0,$$

and therefore,

$$(1 - M^2)^2 \left(\widetilde{\xi}_1 - \frac{\widetilde{\omega} M}{1 - M^2}\right)^2 + (1 - M^2)\|\widetilde{\xi}'\|^2 = \widetilde{\omega}^2.$$

This shows that for $M < 1$ the acoustic part of the characteristic variety is an oblique cone as depicted in Fig. 3a. Both the inclination and the apex angle increase with the Mach number. When the flow is supersonic, $M > 1$, it consists of segments of a double cone, see Fig. 3b. In the subsonic case, for a given ω, there is a bounded set of values for ξ' such that the line defined by (ω, ξ') intersects the characteristic variety. In two-dimensions, for instance, the acoustic modes are cut-on if

$$\xi_2 \in \left[\tfrac{\widetilde{\omega}}{1-M^2}\left(M_2 - \sqrt{1 - M_1^2}\right), \tfrac{\widetilde{\omega}}{1-M^2}\left(M_2 + \sqrt{1 - M_1^2}\right)\right]. \tag{1.12}$$

In the supersonic case there will be a non-empty intersection outside a bounded set. In two dimensions the cut-on condition reads

$$\xi_2 \in \left(-\infty, \tfrac{\widetilde{\omega}}{1-M^2}\left(M_2 - \sqrt{1 - M_1^2}\right)\right] \cup \left[\tfrac{\widetilde{\omega}}{1-M^2}\left(M_2 + \sqrt{1 - M_1^2}\right), +\infty\right).$$

Turbomachinery Boundary Conditions

In the case of a (rotational) turbomachinery configuration, one usually applies the above theory for $n = 2$ to cylinders around the engine axis. More precisely, the coordinate change

$$y = r\vartheta, \quad z = r$$

transforms the Euler flow in an annular duct with constant "hub" and "casing" radii to the three-dimensional flow in

$$\{(x, y, z) \in \mathbb{R}^3 \,|\, r_1 < z < r_2\}$$

as long as the r-components of the flow velocity can be neglected. Moreover, in the case of N blades and a certain interblade phase angle σ, the resulting flow at radius r will have the symmetry

$$q(t, x, y + 2\pi r/N, z) = q(t + \sigma/\omega, x, y, z).$$

The y-components of the wave numbers for which (1.8) must be considered, thus satisfy

$$e^{\mathrm{i}\xi_2(y+2\pi r/N)} = e^{\mathrm{i}\sigma} e^{\mathrm{i}\xi_2 y}.$$

Writing m for the circumferential wave number, we thus have

$$\hat{q}_\omega(x, r, \vartheta) = \sum_{m=N_d \bmod N} \hat{q}_{\omega,m}(x, r) e^{\mathrm{i}m\vartheta}.$$

The cut-on condition for a subsonic flow at radius r is

$$m \in \left[\tfrac{r\widetilde{\omega}}{1-M^2}\left(M_\vartheta - \sqrt{1 - M_x^2}\right), \tfrac{r\widetilde{\omega}}{1-M^2}\left(M_\vartheta + \sqrt{1 - M_x^2}\right)\right].$$

In the cell-centred, finite volume, time-linearised CFD solver discussed here, the boundary conditions are applied at bands of faces whose centre has constant radius. The modal amplitudes $q^j_{\omega,\xi',\mathrm{mod}}$ are computed using the inner cell values along the bands and extrapolated to the bands using the axial wave number ξ for outgoing modes. The modal amplitudes for incoming modes are set to zero. The inverse Fourier transform yields flow states for each face which are then used to define flow states in the ghost cells by extrapolation.

2 ACOUSTIC RESONANCE AND REGULARISATION

The modal decomposition in the previous section is restricted to the case of non-zero group velocity v^1_{g} for all cut-on modes, i.e., we have assumed that the discrimimant Δ is non-zero. If

$$(1 - M_1^2)\|\xi'\|^2 = (\widetilde{\omega} + \xi' \cdot M')^2,$$

then the quadratic equation (1.8) has a real root of algebraic multiplicity 2. However, unless $\xi = 0$, the angular frequency ω is a simple root at the same point. Therefore the eigenspace, i.e., the solution space of (1.2) is one-dimensional.

We regularise the boundary conditions by adding a zeroth order dissipation term to the left-hand side of the model equations. Rather than the linearisation of Eqn. (1.1) we consider

$$\frac{\partial(\delta q)}{\partial t} + \mathrm{div}\left[\left.\frac{\partial F}{\partial q}\right|_q \delta q\right] + \varepsilon\delta q = 0, \tag{2.1}$$

where $\varepsilon > 0$ is a small regularisation parameter. The corresponding equation in dual variables thus reads

$$\left(\omega - \mathrm{i}\varepsilon + \sum_k \xi_k A^k\right) \hat{q}_{\omega,\xi} = 0. \tag{2.2}$$

If ω is replaced with $\omega - \mathrm{i}\varepsilon$, the formulas of Section 1 essentially remain valid. The crucial difference, however, is that there are no longer cut-on modes. More presicely, given real ω and ξ', Eqn. (2.2) will have only trivial solutions for real ξ_1 since, otherwise, $\omega - \mathrm{i}\varepsilon$ would be a non-real eigenvalue of a symmetric operator. Since all eigenvalues ξ_1 have non-zero imaginary part, all eigenspaces correspond to either incoming or outgoing modes.

If ξ is non-zero and $\xi_{1,\mathrm{a},\pm}(q,\omega,\xi')$ corresponds to a cut-on acoustic mode of the original system, then ω is locally a smooth holomorphic function of ξ. Moreover, if locally $\frac{\partial\omega}{\partial\xi_1}$ is non-zero, then the generalised eigenvalue ξ_1 is, locally, a holomorphic function of ω. Using the Cauchy-Riemann equations, we infer

$$\begin{aligned}
\operatorname{sign} \operatorname{Im} \xi_{1,\mathrm{a},\pm}(q,\omega - \mathrm{i}\varepsilon,\xi') &= -\operatorname{sign} \frac{\partial \operatorname{Im} \xi_{1,\mathrm{a},\pm}}{\partial \operatorname{Im}\omega}\Big|_{(q,\omega,\xi')} \\
&= -\operatorname{sign} \frac{\partial \operatorname{Re} \xi_{1,\mathrm{a},\pm}}{\partial \operatorname{Re}\omega}\Big|_{(q,\omega,\xi')} \\
&= -\operatorname{sign} \frac{\partial \omega}{\partial \xi_{1,\mathrm{a},\pm}}\Big|_{(\xi_{1,\mathrm{a},\pm}(q,\omega,\xi'),\xi')} \\
&= \operatorname{sign} v_{\mathrm{g}}^1.
\end{aligned} \tag{2.3}$$

Therefore, defining the acoustic normal wavenumbers by the analytic continuation of the formulas given in Eqn. (1.9), we preserve the propagation direction in the sense that, e.g, right-running cut-on modes become right-running cut-off modes. Denoting by $\sqrt{z}$ the principal branch of the complex square root, it is now easy to verify that the analytic continuation of (1.9) is

$$\xi_{1,\mathrm{a},\pm} = (M_1 \mp \sqrt{\Delta}) \left(\frac{\widetilde{\omega} - \mathrm{i}\widetilde{\varepsilon} + \xi' \cdot M'}{1 - M_1^2}\right),$$

where

$$\widetilde{\varepsilon} = \frac{\varepsilon}{a}, \quad \Delta = 1 - \frac{(1 - M_1^2)\|\xi'\|^2}{(\widetilde{\omega} - \mathrm{i}\widetilde{\varepsilon} + \xi' \cdot M')^2}.$$

The definition of the right-eigenvectors carries over to the modified model problem. In particular, the acoustic eigenvectors are replaced with $r_{\mathrm{a},\pm}(q,\omega - i\varepsilon,\xi')$, cf. Eqn. (1.10). We emphasize, that for $\varepsilon > 0$, the above terms are holomorphic for all ω, ξ', including the acoustic resonance points.

3 ANALYSIS OF TURBOMACHINERY FLUTTER

To illustrate the modification of the boundary condition we will use the so-called tenth standard configuration (SC10) [2]. This configuration is a two-dimensional compressor test case consisting of a cambered NACA 0006 cascade at subsonic and transonic flow conditions. The eigenmode for which flutter stability is analysed corresponds to a rigid body rotation about the blade center. Flow conditions and reduced eigenfrequencies are summarised in Table 1. Observe that the reduced frequencies k are computed using the full chord c and the flow speed at the inlet U_{inlet}, i.e.,

$$\omega_{\mathrm{red}} = \frac{\omega c}{\|U_{\mathrm{inlet}}\|}.$$

Testcase	SC10 subsonic	SC10 transonic
Inflow Mach number	0.7	0.8
Inflow angle	$55°$	$58°$
Outflow Mach number	0.446	0.443
Outflow angle	$40.1°$	$41.1°$
Reduced frequency	1	0.5
Upstream acoustic resonances	$-26.9°$	$-14.5°$
	$117.1°$	$100.8°$
Downstream acoustic resonances	$-31.8°$	$-17.8°$
	$59.8°$	$33.7°$

Table 1: Flow conditions, frequencies and acoustic resonances.

The steady isentropic Mach number distributions on the blade are shown in Fig. 4. Both the subsonic and the transonic background mean flow conditions, used for the linearised flutter simulations below, agree well with reference results obtained with a different flow solver, [16].

The flutter predictions using different values for the regularisation parameter ε are shown in Figs. 5 and 6. The value of ε is non-dimensionalised using the sound speed at the inlet and the chord length and thus equals, up to the inlet Mach number, the negative imaginary part of the modified reduced frequency. The results for $\varepsilon = 10^{-3}$ have been validated against reference results in previous publications by the authors [4, 17] and show good agreement with results obtained with a different solver [15, 16].

However, as ε is increased, the damping curve becomes "smoother". This can be seen, for both the subsonic as the transonic configuration, near the interblade phase angles with minimal damping, which are close to the downstream acoustic resonance points $59.8°$ and $33.7°$. The zooms also show that the choice of ε above 10^{-1} can have a significant impact on the prediction of the flutter stability and is therefore discouraged.

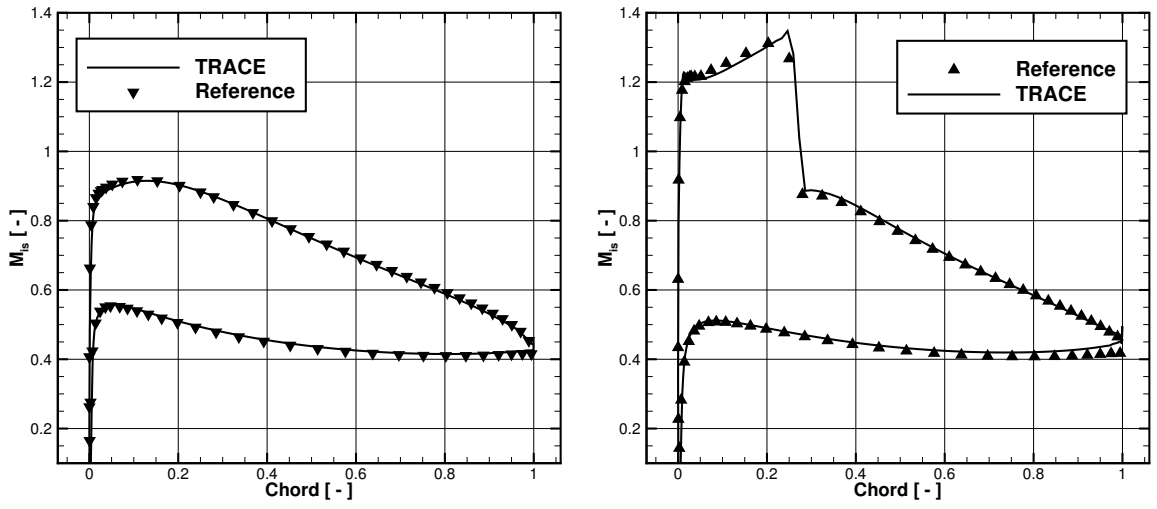

(a) Subsonic Case (b) Transonic Case

Figure 4: Comparison of steady solution with references given in [15]

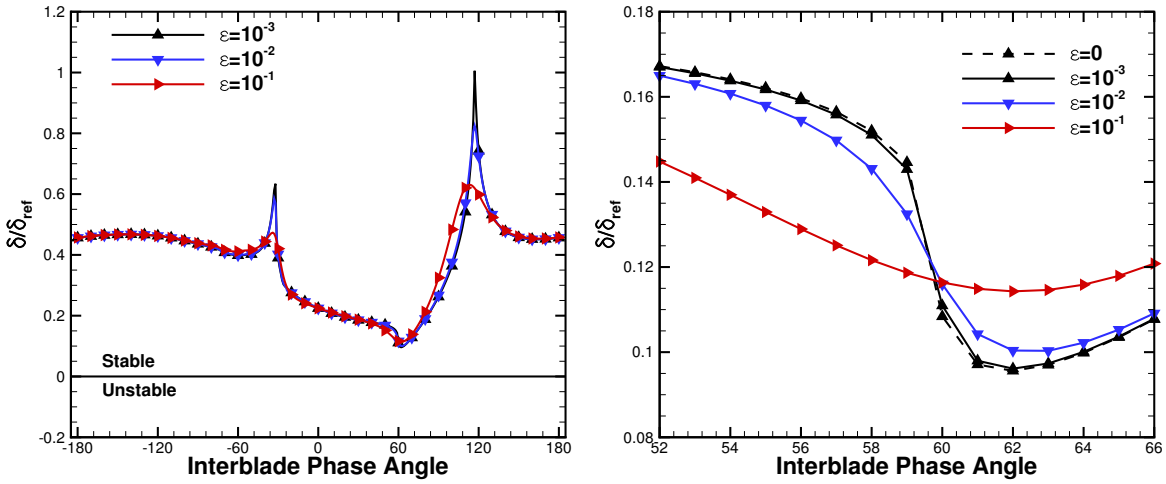

(a) Normalised aerodynamic damping over interblade phase angle.

(b) Minimal damping region

Figure 5: Damping results for the subsonic case.

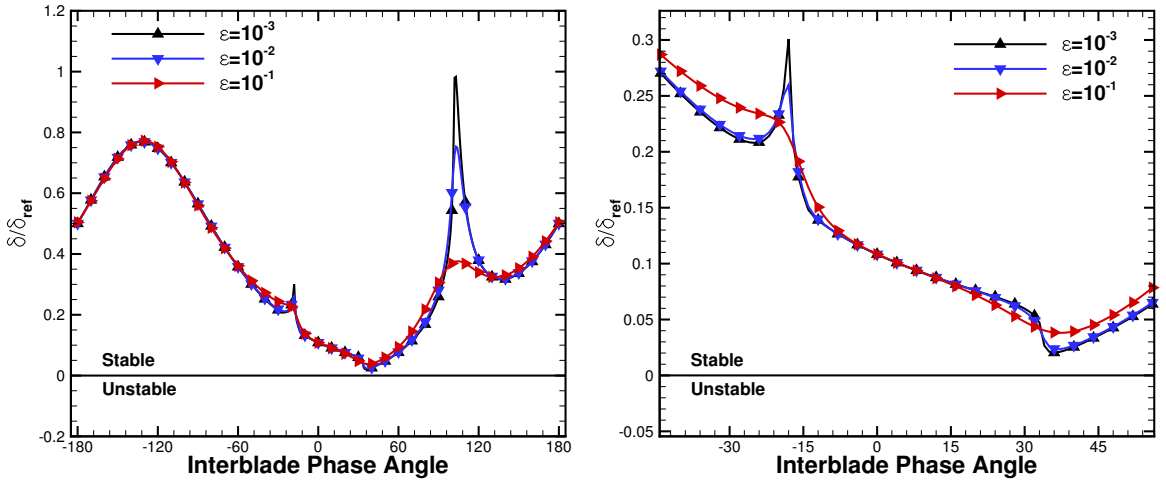

(a) Normalised aerodynamic damping over interblade phase angle.

(b) Minimal damping region

Figure 6: Damping results for the transonic case.

4 INTERPRETATION OF THE REGULARISATION

Let us study the behaviour of the regularised spectral projection P_{inc} as ε tends to infinity. Denoting by χ_Λ the characteristic function of a complex set Λ, we can write the regularised projection onto the incoming modes as

$$P_{\text{inc}} = \chi_{\{\operatorname{Im}\xi_1<0\}}\left(-(A^1)^{-1}\left(\omega - \mathrm{i}\varepsilon + \xi' A'\right)\right)$$

Observe that

$$\| -(A^1)^{-1}\left(\omega - \mathrm{i}\varepsilon + \xi' A'\right) \| \leq \varepsilon \|A^{-1}\| + \text{const}\,.$$

Therefore, for an appropriate $R > 0$ and sufficiently large ε, the contour γ_ε, depicted in Fig. 7, encircles all eigenvalues ξ_1 with negative imaginary part anticlockwise. Using holomorphic

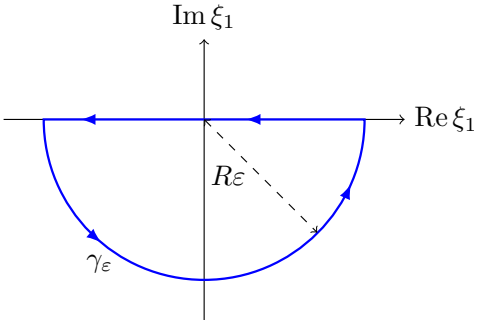

Figure 7: Closed contour encircling the acoustic normal wave numbers of the regularised system anticlockwise.

.

functional calculus, we have

$$\begin{aligned} P_{\text{inc}} &= \frac{1}{2\pi \mathrm{i}} \int_{\gamma_\varepsilon} \left(\xi_1 + (A^1)^{-1}(\omega - \mathrm{i}\varepsilon + \xi' A')\right)^{-1} d\xi_1 \\ &= \frac{1}{2\pi \mathrm{i}} \int_{\gamma_1} \left(z + (A^1)^{-1}(-\mathrm{i} + \varepsilon^{-1}(\omega + \xi' A'))\right)^{-1} dz, \end{aligned} \tag{4.1}$$

where we have made the substitution $\xi_1 = \varepsilon z$. Since

$$-(A^1)^{-1}(-\mathrm{i} + \varepsilon^{-1}(\omega + \xi' A'))$$

has no real eigenvalues and converges uniformly to $\mathrm{i}(A^1)^{-1}$ along γ_1 for $\varepsilon \to \infty$, it follows that P_{inc} converges to the spectral projection

$$\chi_{\{\operatorname{Im} z<0\}}(\mathrm{i}(A^1)^{-1}) = \chi_{\{\operatorname{Re} z<0\}}(A^1).$$

Therefore, in the limit $\varepsilon \to +\infty$, the regularised boundary conditions converge to characteristic boundary conditions. This is confirmed by numerical experiments, see Fig. 8. As the parameter ε is increased, the results for the aerodynamic damping approach the curve which is obtained by using one-dimensional, characteristics based boundary conditions. Note that for this numerical experiment, the modified normal wave number has been replaced by 0 in the extrapolation of the outgoing mode amplitudes to the ghost cells.

5 DISCUSSION

So far, we have studied only a two-dimensional test case and two-dimensional boundary conditions which raises the question of the relevance for real three-dimensional turbomachinery configurations. Therefore, consider a computational domain representative of an annular duct in a real engine. Although two-dimensional (or even characteristic one-dimensional) non-reflecting boundary conditions are still predominantly used for turbomachinery simulations, three-dimensional non-reflecting boundary conditions have been developed by several authors [18, 19]. For a general mean flow distribution, the eigenmodes can no longer been computed explicitly. Rather, one performs a numerical spectral decomposition using e.g. appropriate LAPACK routines [20, 11]. In three dimensions, the equivalent of Eqn. (1.2), can be written in the form

$$(\mathrm{i}(\omega + \xi A^x + mC) + B\frac{\partial}{\partial r} + D)\hat{q}_{\omega,\xi,m}(r) = 0, \tag{5.1}$$

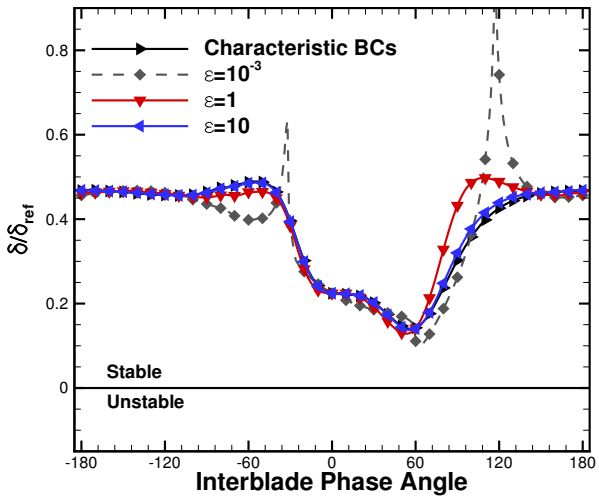

Figure 8: Normalised aerodynamic damping over interblade phase angle for subsonic case and large values for ε.

with suitable boundary conditions at the hub and tip radii, $r_{\min}$, $r_{\max}$, [20]. In case the mean flow is purely axial, the pressure harmonics satisfy

$$\left(-\frac{\partial^2}{\partial r^2} - \frac{1}{r}\frac{\partial}{\partial r} + \xi_x^2 + \frac{m^2}{r^2} - (\widetilde{\omega} + \xi_x M_x)^2\right) \widehat{p}_{\omega,\xi,m}(r) = 0, \tag{5.2}$$

together with Neumann boundary conditions at $r_{\min}$ and $r_{\max}$. Eqn. (5.2) may thus be written in the form

$$\left(L(m) + \xi_x^2 - (\widetilde{\omega} + \xi_x M_x)^2\right) \widehat{p}_{\omega,\xi,m}(r) = 0$$

where $L(m)$ is an elliptic self-adjoint eigenvalue problem (with respect to the Riemannian metric $g(r) = r^2$) depending on m. From its discrete eigenvalues $(\lambda_n(m))_{n\geq 0}$, we can thus determine the relation between the axial wavenumber and $\widetilde{\omega}$ for all radial and circumferential mode orders, (n, m):

$$\lambda_n(m) + \xi_x^2 + (\widetilde{\omega} + \xi_x \cdot M_x)^2 = 0. \tag{5.3}$$

Viewing m as a continuous parameter, we can thus plot the generalisation of the two-dimensional characteristic varieties for each radial mode order n. Figure 9 shows the surface defined by (5.3) for the radial mode orders $n = 0, 1, 2$. Here, $M_x = 0.5$ and $r_{\min} = 1$, $r_{\max} = 2$. The resulting surfaces resemble the upper sheets of an oblique two-surface hyperboloid except for $n = 0$ in which case the surface is a slightly deformed oblique cone. In many cases the three-dimensional characteristic variety for $n = 0$ is very close to the two-dimensional one. For the above parameters the two-dimensional characteristic variety at $r = \frac{1}{2}(r_{\min} + r_{\max})$ is nearly identical to the three-dimensional one for $n = 0$, see Fig. 10.

If acoustic resonance occurs for certain values of (ω, ξ_x, m, n), then ξ_x is a double zero of Eqn. (5.3), whereas ω is a simple one. Hence, similar arguments as in the two-dimensional case show that the geometric multiplicity of the generalised eigenvalue problem for ξ_x is 1. This shows that the modal decomposition has to be regularised in the three-dimensional case as well. In their implementations of three-dimensional non-reflecting boundary conditions [19], the authors perform a numerical eigenvalue analyis of (5.1) where ω is replaced with $\omega - \mathrm{i}\varepsilon$ and ε is typically set to $10^{-3} a_{\mathrm{ref}}/l_{\mathrm{ref}}$. Here a_{ref}, l_{ref} denote reference sound speed and length,

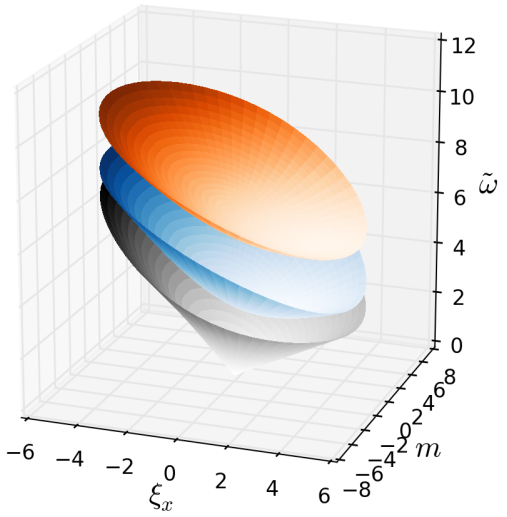

Figure 9: Three-dimensional characteristic variety for radial mode orders 0 (grey), 1 (blue), and 2 (orange).

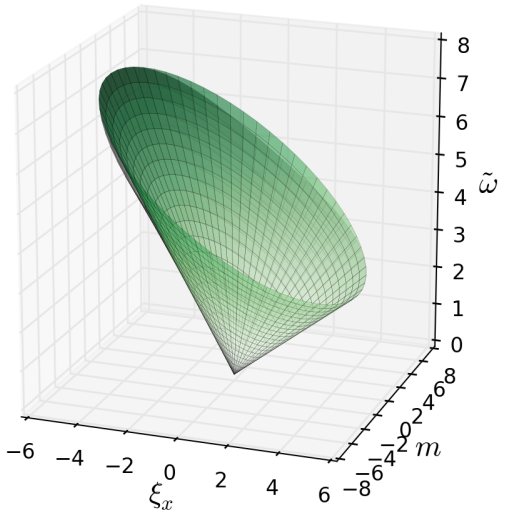

Figure 10: Three-dimensional Characteristic variety for radial mode orders 0 (grey) compared to the two-dimensional one at $r = \frac{1}{2}(r_{\min} + r_{\max})$ (green).

respectively. The regularisation allows to circumvent the numerical computation of the group velocity, as pointed out in [11]. One can use the sign of $\operatorname{Im} \xi_x$ to determine the propagation direction of the modes.

Acoustic resonance occurs when one of the characteristic varieties has vanishing slope in the ξ_x-direction. For a given frequency, this can happen at several radial orders, although in practice, for only a few low values of n there exist cut-on modes, i.e., the plane $\omega = \text{const}$ intersects only a few of the hyperboloids in Fig. 9. Therefore, one can expect that the use

of two-dimensional boundary conditions for a three-dimensional configuration might suppress acoustic resonance for some non-zero radial mode orders but will show qualitatively similar results as far as the acoustic resonance for $n = 0$ is concerned.

This is illustrated by the flutter analysis of a turbine blade carried out in [19]. The test case represents a low pressure turbine blade of a modern aeroengine. As can be seen in Figure 11, the use of three-dimensional instead of two-dimensional non-reflecting boundary conditions has a significant impact on the unsteady pressure distribution on the blade. However, the aerodynamic damping is very insensitive to the choice of boundary conditions, in particular near the resonance point located between $-30°$ and $-20°$.

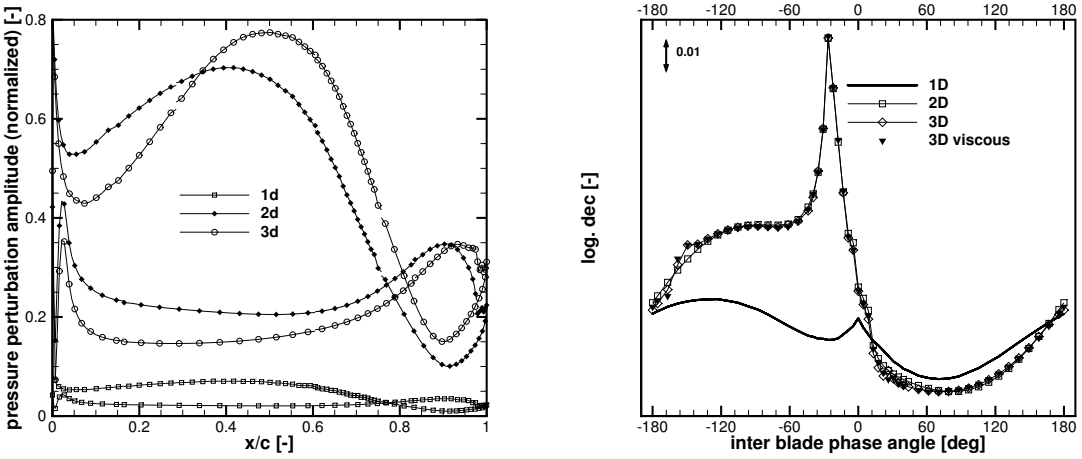

(a) Pressure amplitude over chord for $\sigma = -88°$.

(b) Damping curve.

Figure 11: Flutter analysis of a turbine blade with 1D, 2D, and 3D non-reflecting boundary conditions. From [19].

CONCLUSIONS

In this paper, a regularisation of the non-reflecting boundary conditions for unsteady turbomachinery flows has been investigated. The regularisation is necessary in order to ensure that the spectral projections onto outgoing along incoming modes remain bounded. The idea is to apply the usual theory of non-reflecting boundary conditions to the Euler equations modified by a small dissipation term which is controlled by some parameter ε. As the additional dissipation increases the resulting flutter curves become smoother. A choice of $\varepsilon = 10^{-3}$ with respect to the reference frequency has been shown to be a reasonable choice for the turbomachinery test cases presented in this paper. As ε grows, the boundary conditions approach the one-dimensional characteristics based boundary conditions.

The issue of acoustic resonance occurs for both two-dimensional and three-dimensional non-reflection boundary conditions. It is suspected that using two-dimensional boundary conditions for a three-dimensional turbomachinery configuration might smooth out singularities in the damping curve which are related to acoustic resonance modes of non-zero radial order.

ACKNOWLEDGEMENTS

This study was conducted as part of the joint research programme *AG-Turbo 2020*. The authors gratefully acknowledge financial supported from the German Federal Ministry for Economic Affairs and Energy under grant number 03ET2012G.

NOMENCLATURE

a	speed of sound
A^i	flux Jacobian in the x^i-direction
A^1, A'	normal and tangential flux Jacobians
e_t	total (specific) energy
f	frequency
h_t	total (specific) enthalpy
k	modal stiffness
m	modal mass, circumferential wave number
$\vec{M} = U/a$	Mach vector
M^1, M'	normal Mach number and tangential Mach vector
N	number of blades
N_d	nodal diameter
$\vec{n}$	unit normal vector (pointing out of the flow domain)
p	pressure
q	flow state
q^s	modal displacement
s	specific entropy
(x, r, ϑ)	cylindrical coordinates
$x^1, x' = (x^2, \ldots, x^n)$	normal and tangential coordinates
U	flow velocity
W_cyc	aerodynamic work per cycle
δ	logarithmic decrement of aerodynamic damping
γ	specific heat ratio
κ	aerodynamic stiffness coefficient
	structural eigenmode (mode shape)
ρ	density
σ	interblade phase angle
χ_Λ	characteristic function of a set $\Lambda \subset \mathbb{C}$
ω	angular frequency ($= 2\pi f$)

REFERENCES

[1] R. Kielb, "CFD for turbomachinery unsteady flows - an aeroelastic design perspective," in *Aerospace Sciences Meetings*, American Institute of Aeronautics and Astronautics, 2001.

[2] T. H. Fransson and J. M. Verdon, "Updated report on Standard Configurations for the Determination of unsteady Flow Through Vibrating Axial-flow Turbomachine-Cascades," Tech. Rep. TRITA/KRV/92.009, KTH, Stockholm, 1992.

[3] K. C. Hall and W. S. Clark, *Unsteady Aerodynamics, Aeroacoustics, and Aeroelasticity of Turbomachines and Propellers*, ch. Calculation of Unsteady Linearized Euler Flows in

Cascades Using Harmonically Deforming Grids, pp. 195–212. New York, NY: Springer New York, 1993.

[4] H.-P. Kersken, C. Frey, C. Voigt, and G. Ashcroft, "Time-Linearized and Time-Accurate 3D RANS Methods for Aeroelastic Analysis in Turbomachinery," *J. Turbomach.*, vol. 134, no. 5, pp. 051024–051024, 2012.

[5] G. Kahl, *Aeroelastic effects of mistuning and coupling in turbomachinery bladings*. PhD thesis, École polytechnique fédérale de Lausanne, 2002.

[6] J. J. Waite and R. E. Kielb, "Physical understanding and sensitivities of low pressure turbine flutter," *Journal of Engineering for Gas Turbines and Power*, vol. 137, pp. 012502–012502, Aug. 2014.

[7] T. R. Camp, "A study of acoustic resonance in a low-speed multistage compressor," *Journal of Turbomachinery*, vol. 121, pp. 36–43, Jan. 1999.

[8] B. Hellmich and J. R. Seume, "Causes of acoustic resonance in a high-speed axial compressor," *Journal of Turbomachinery*, vol. 130, pp. 031003–031003, May 2008.

[9] B. Engquist and A. Majda, "Absorbing boundary conditions for the numerical simulation of waves," *Math. Comp.*, vol. 31, pp. 629–651, May 1977.

[10] M. B. Giles, "Non-reflecting boundary conditions for the Euler equations," tech. rep., MIT Dept. of Aero. and Astr., 1988. CFDL Report 88-1.

[11] P. Moinier and M. Giles, "Eigenmode analysis for turbomachinery applications," *Journal of Propulsion and Power*, vol. 21, no. 6, pp. 973–978, 2005.

[12] K. Friedrichs and P. Lax, "Systems of conservation equations with a convex extension," *Proceedings of the National Academy of Sciences of the United States of America*, vol. 68, no. 8, 1971.

[13] M. Taylor, *Partial Differential Equations I: Basic Theory*. Applied Functional Analysis: Applications to Mathematical Physics, Springer, 1996.

[14] R. L. Higdon, "Initial-boundary value problems for linear hyperbolic systems," *SIAM Rev.*, vol. 28, pp. 177–217, June 1986.

[15] P. J. Petrie-Repar, A. M. McGhee, and P. A. Jacobs, "Three-dimensional viscous flutter analysis of standard configuration 10," in *Proceedings of the ASME Turbo Expo 2007*, 2007.

[16] RPMTurbo Pty. Ltd., "RPMTurbo Standard Configuration 10." http://rpmturbo.com/testcases/sc10/index.html, 2005-2014.

[17] G. Ashcroft, C. Frey, and H.-P. Kersken, "On the development of a harmonic balance method for aeroelastic analysis," in *6th European Conference on Computational Fluid Dynamics (ECFD VI)*, 2014.

[18] P. Moinier, M. B. Giles, and J. Coupland, "Three-dimensional nonreflecting boundary conditions for swirling flow in turbomachinery," *Journal of Propulsion and Power*, vol. 23, no. 5, pp. 981–986, 2007.

[19] H.-P. Kersken, G. Ashcroft, C. Frey, N. Wolfrum, and D. Korte, "Nonreflecting boundary conditions for aeroelastic analysis in time and frequency domain 3D RANS solvers," in *Proceedings of ASME Turbo Expo 2014*, 2014.

[20] V. Golubev and H. Atassi, "Sound propagation in an annular duct with mean potential swirling flow," *Journal of Sound and Vibration*, vol. 198, no. 5, pp. 601–616, 1996.